Article

Allosteric Inhibitors Have Distinct Effects, but Also Common Modes of Action, in the HCV Polymerase

Brittny C. Davis,[1] Jodian A. Brown,[1] and Ian F. Thorpe[1,*]
[1]Department of Chemistry and Biochemistry, University of Maryland Baltimore County, Baltimore, Maryland

ABSTRACT The RNA-dependent RNA polymerase from the Hepatitis C Virus (gene product NS5B) is a validated drug target because of its critical role in genome replication. There are at least four distinct allosteric sites on the polymerase to which several small molecule inhibitors bind. In addition, numerous crystal structures have been solved with different allosteric inhibitors bound to the polymerase. However, the molecular mechanisms by which these small molecules inhibit the enzyme have not been fully elucidated. There is evidence that allosteric inhibitors alter the intrinsic motions and distribution of conformations sampled by the enzyme. In this study we use molecular dynamics simulations to understand the structural and dynamic changes that result when inhibitors are bound at three different allosteric binding sites on the enzyme. We observe that ligand binding at each site alters the structure and dynamics of NS5B in a distinct manner. Nonetheless, our studies also highlight commonalities in the mechanisms of action of the different inhibitors. Each inhibitor alters the conformational states sampled by the enzyme, either by rigidifying the enzyme and preventing transitions between functional conformational states or by destabilizing the enzyme and preventing functionally relevant conformations from being adequately sampled. By illuminating the molecular mechanisms of allosteric inhibition, these studies delineate the intrinsic functional properties of the enzyme and pave the way for designing novel and more effective polymerase inhibitors. This information may also be important to understand how allosteric regulation occurs in related viral polymerases and other enzymes.

INTRODUCTION

The Hepatitis C virus (HCV) infects ~3% of the world's population, making it a global health problem (1–3). HCV possesses a positive stranded RNA genome that can be immediately translated once it infects a host cell. The resulting polyprotein is cleaved to give rise to four structural proteins (core, E1, E2, and p7) and six nonstructural proteins NS2, NS3, NS4A, NS4B, NS5A, and NS5B) (1,3). NS5B is the RNA-dependent RNA polymerase (see Fig. 1) that replicates the HCV genome and is a validated drug target (3–5).

To function, NS5B is believed to interchange between at least two conformations: a closed conformation required for de novo initiation, and an open conformation required for elongation of the newly transcribed RNA strand (6–8). In the closed conformation, the thumb and fingers domains are rotated closer toward each other such that residues within the template channel are primed for initiation, while in the open conformation the thumb and fingers domains are positioned further apart such that the RNA duplex channel widens to accommodate nascent double-stranded transcripts (7,8).

Previously (9), we used molecular simulations to identify a fully closed NS5B conformation that we proposed to be suitable for de novo initiation, based on its resemblance to initiation complexes of polymerases from related viruses such as bacteriophage ϕ6 or poliovirus (10). This conformation is stabilized by the presence of two magnesium ions in the palm domain and absence of the 60 C-terminal residues, which allows for increased interaction between the fingers and thumb domain via new hydrogen bonds (9). It is believed that the C-terminus is necessary for docking the polymerase to the endoplasmic reticulum membrane in vivo, as it is extremely hydrophobic. In the absence of the endoplasmic reticulum membrane, the C-terminus can become lodged between the fingers and thumb domains, which has been shown to significantly decrease polymerase function in vitro (11). Our previous computational studies demonstrated that the C-terminus disrupts interactions between the thumb and fingers domains, significantly decreasing flexibility and limiting conformational sampling of NS5B (9).

A considerable effort has been made to identify inhibitors that target the HCV polymerase. Two broad classes of inhibitors that have been widely investigated as potential therapeutics: active site and allosteric inhibitors (1,12). The active site inhibitors are based on either nucleoside or pyrophosphate scaffolds and function as chain terminators of the nascent RNA transcript (13). Nucleoside inhibitors act via preventing additional nucleotides from being incorporated, while pyrophosphate analogs coordinate the divalent ions required for catalysis (e.g., magnesium or manganese ions). This coordination prevents the departure of the pyrophosphate group and obstructs binding of additional nucleotides (13,14). In contrast to the active site inhibitors,

Submitted December 1, 2014, and accepted for publication March 4, 2015.
*Correspondence: ithorpe@umbc.edu
Editor: Michael Feig.

0006-3495/15/04/1785/11 $2.00
http://dx.doi.org/10.1016/j.bpj.2015.03.005

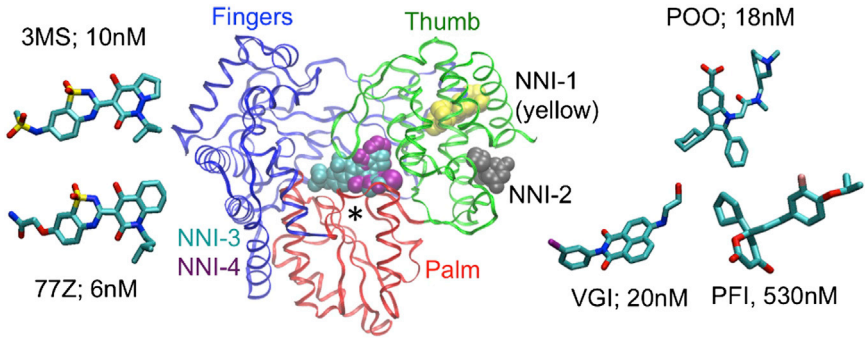

FIGURE 1 The RNA polymerase (NS5B) from the hepatitis C virus showing locations of allosteric sites and inhibitor structures. (*Blue*) Fingers, (*red*) palm, and (*green*) thumb domains. The active site is marked by an asterisk (*). Of the four allosteric binding sites, three were examined in this study: NNI-1, NNI-2, and NNI-3. Structures for each ligand are shown in addition to their respective IC_{50} values. To see this figure in color, go online.

allosteric inhibitors (commonly referred to as nonnucleoside inhibitors or NNIs) bind distal to the polymerase active site.

Of the four confirmed allosteric binding sites, two are located in the thumb domain (NNI-1 and NNI-2) and two in the palm domain (NNI-3 and NNI-4) (Fig. 1) (15–24). We will refer to NNI-1 and -2 as "thumb inhibitors" while NNI-3 and -4 will be referred to as "palm inhibitors". NNIs encompass diverse chemical scaffolds and exhibit mechanisms of action that have not been conclusively elucidated. However, some studies suggest that palm NNIs like benzodiazepine derivatives inhibit initiation while thumb NNIs such as benzimidazole derivatives inhibit an early phase of replication that occurs after initiation, but precedes elongation (23,25–27). Previously, we used molecular dynamics (MD) simulations to demonstrate that an NNI-2 inhibitor forces the enzyme to adopt a hyperclosed conformation (28). The hyperclosed conformation is distinct from the fully closed conformation that we previously characterized for an inhibitor-free enzyme (9), as it has a template channel that is likely to be too narrow to accommodate an RNA strand. While the fully closed conformation may be ideal for de novo initiation, it is likely that the hyperclosed conformation represents a nonfunctional conformational state (28).

In this work, MD simulations were employed to resolve the molecular mechanisms of inhibition for palm and thumb inhibitors (Fig. 1). We provide evidence that the structure and dynamics of ligand-bound enzymes are significantly different from those of the free enzymes and that these differences may play a role in mediating the inhibitory effects of these molecules. While our observations indicate that palm and thumb inhibitors induce distinct structural and dynamic effects, both classes of inhibitors have the common feature of disrupting the equilibrium distribution of conformations sampled by the enzyme in ways that would tend to reduce its activity.

MATERIALS AND METHODS

Simulation conditions

Crystal structures of the genotype 1b HCV RNA polymerase (NS5B) from the Protein Data Bank (PDB) with the following PDB codes were used as the initial coordinates (location of the allosteric binding site is in parentheses): PDB: 2BRL (NNI-1), PDB: 2HAI (NNI-2), PDB: 2WHO (NNI-2), PDB: 3CO9 (NNI-3), and PDB: 3HHK (NNI-3) (19,21–24). The PDB: 2BRL crystal structure did not contain residues 22–35 (the Δ1 loop near the ligand binding site) or 148–152 (part of the Δ2 loop). Coordinates for these residues were taken from PDB: 2WHO, placed into the PDB: 2BRL structure and energy-minimized. Visual inspection confirmed that these residues were successfully incorporated. An RMSF profile of the residues in the Δ1 loop is provided in Fig. S1 in the Supporting Material to demonstrate that there are no abnormal motions that occur in this region when compared to the other structures. Simulations with PDB: 2WHO were carried out in a previous study (28); however, some of the results are presented again here for comparison. Each structure was simulated in a free and a ligand-bound state. Ligands were parameterized using the protocol outlined in Vanommesleaghe et al. (29), and ligand parameter files are available upon request.

Descriptions and abbreviations applied to each simulated system are listed in Table 1. Previously, we demonstrated that the presence of the magnesium ions and deletion of the 60 C-terminal residues facilitates conformational sampling (9). These conditions have been applied to each of the systems described in this study. Each structure was placed in a truncated octahedral unit cell that was larger than the protein by at least 10 Å in each dimension, generating unit cells with an edge length of at least 93 Å. TIP3P (30) water molecules and 19 chloride ions were added to the unit cell to solvate and neutralize the system, respectively. All water molecules that overlapped with protein, ligand, or ions were

TABLE 1 Description of simulated systems and associated abbreviations

System abbreviation	Enzyme structure	Description	Conventional MD/TAMD/total
1	PDB: 2BRL		460/340/800
1:POO	PDB: 2BRL	L: POO (NNI-1)	0/500/500
2	PDB: 2WHO		400/0/400[a]
2:PFI	PDB: 2WHO	L:PFI (NNI-2)	0/500/500
2:VGI	PDB: 2WHO	L: VGI (NNI-2)	400/0/400[a]
3	PDB: 2HAI	mutations: L47Q, F101Y, K114R	500/200/700
3:PFI	PDB: 2HAI	mutations: L47Q, F101Y, K114R L: PFI (NNI-2)	60/440/500
4	PDB: 3CO9		510/200/710
4:3MS	PDB: 3CO9	L: 3MS (NNI-3)	500/200/700
5	PDB: 3HHK		500/400/900
5:77Z	PDB: 3HHK	L: 77Z (NNI-3)	0/500/500

All systems contain 531 amino acids and magnesium ions. L = ligand-bound (NNI-site). Totals are underlined.
[a]Values obtained from a previous study (28).

deleted, resulting in simulation systems that contained ~60,000 atoms each.

Simulations were performed using the CHARMM27 protein force field and the CHARMM general force field (CGenFF, Ver. 2b6) (29–32) using the software NAMD, Ver. 2.9 (33). Minimization of the solvated system was carried out using NAMD for 1000 steps using the conjugate gradient method and applying periodic boundary conditions. All bonds to hydrogen atoms were constrained using the SHAKE algorithm, and electrostatic interactions were calculated by the particle-mesh Ewald method. A distance of 9 Å was used for the Coulomb cutoff and 11.4 Å for the nonbonded pair list. Minimization was followed by 2,500,000 steps of simulation in the NVT ensemble at 300 K using NAMD and a 2-fs integration time step. Temperature was maintained via velocity reassignment every 100 steps, during which the positions of α-carbons was restrained using force constants of 10 kcal(mol^{-1} Å^{-2}).

The restrained NVT was followed by simulations in the NPT ensemble at 300 K for 2,500,000 steps using Berendsen pressure coupling at 1.01 bar with a relaxation time of 100 fs. The temperature was maintained via velocity reassignment every 100 steps. Finally, production NVT simulations were performed using the same conditions as the original NVT simulations, except that temperature was maintained using a Langevin thermostat with a damping coefficient of 1 ps^{-1} applied to heavy atoms. The pressure was checked every 10 ns to confirm that it remained within reasonable range of 1.01 bar.

Table 1 provides a description of each system and lists how much conventional MD or temperature-accelerated MD (TAMD) data were generated for each structure. For simulations with TAMD data available, the final 200 ns of TAMD data were used for analysis (see TAMD discussion in next section). Otherwise, the final 200 ns of conventional MD were analyzed.

TAMD

TAMD (34) was performed to complement the conventional MD simulations in order to increase the sampling of open and closed conformations. TAMD requires the selection of a collective variable (CV). A CV is a combination of atomic coordinates that can act as a reaction coordinate to be restrained or, in our case, driven using TAMD. We chose the interdomain angle θ (see Results and Discussion) as the single CV. A friction coefficient of 10 ps^{-1} was used for the CV and its temperature was set to 32 k_BT. TAMD was implemented via a Tcl language interface to NAMD provided by Dr. Cameron Abrams (Abrams and Vanden-Eijnden (35)).

While intended to enhance sampling, we observed that the sampling and dynamics of θ were not significantly altered in the TAMD simulations. We believe this is due to the fact that, while θ is a good progress variable for the conformational changes sampled by NS5B, it is not a good reaction coordinate. However, employing TAMD was still useful in providing additional sampling that allowed for a more comprehensive representation of the enzyme free energy landscape. Our observations indicate that the description of the free energy landscape provided by TAMD is essentially the same as that obtained from conventional MD. Thus, results from TAMD and conventional MD are presented on equivalent footing in these studies. A complete discussion of the TAMD simulations is provided in Text S2 in the Supporting Material.

Measures of conformational sampling

To quantify the degree of closure, we employed two structural metrics, as follows.

Interdomain angle (θ)

The interdomain angle occurs at the intersection of the fingers, palm, and thumb domains. It was computed by determining the angle between the centers of mass of each domain. The residue composition of each domain is defined according to Lesburg et al. (36): the fingers domain contains residues 1–188 and 227–287, the palm domain contains residues 189–226, and 288–370, and the thumb domain contains residues 371–531.

Template channel width

The template channel width is calculated by measuring the distance between the centers of mass of residues 139 and 405. Smaller angles and narrower widths correspond to a more closed enzyme. Values of 70° for θ and 20 Å for the template channel width represent the demarcation between open and closed conformations.

These values were chosen because they seem to give a natural separation between the distinct conformational minima displayed for the different simulations, as shown in Fig. 2. Conformations for which both criteria are not satisfied are classified as intermediate. Thus, the total population in the open and closed states does not necessarily equal to 100% (see Results and Discussion below). It should be noted that our definition of open and closed conformations differs from that employed by Gong and Peersen (37). These authors defined the closed state as a conformation where key active-site residues are aligned to adopt catalytically competent conformations, while in the open state the active-site residues are not aligned for catalysis. Thus, the definition employed by these authors describes the local vicinity of the active site while the definition employed in this work describes the overall enzyme structure. We note that the definition employed here is consistent with that employed by other authors who discuss these conformational states in the context of the global enzyme structure (8,38–40).

Root-mean-square fluctuations

The root-mean-square fluctuation (RMSF) was calculated to determine the localized flexibility of the enzyme using Eq. 1. RMSF is calculated by subtracting the average position $\tilde{x}_i$ of each atom from its instantaneous position $x_i(t_j)$, as

$$RMSF_i = \sqrt{\frac{\sum_{t_j}^{T}\left[x_i(t_j) - \tilde{x}_i\right]^2}{T/dt}} \tag{1}$$

$$\Delta RMSF_i = x_{F,i} - x_{L,i}, \tag{2}$$

where T is the total length of the trajectory, t_j is a time point, and dt is the time interval at which coordinates were written out. RMSF values for the ligand-bound structures were subtracted from those of the corresponding free structures to generate $\Delta RMSF$ values, as shown in Eq. 2. $\Delta RMSF$ values >0 indicate that free ($x_{F,i}$) structures are more flexible while those <0 indicate that ligand-bound ($x_{L,i}$) structures are more flexible.

Hydrogen-bond analysis

Hydrogen bonds were detected with the CORMAN module in the software CHARMM (http://www.charmm.org/) using the default settings, which specify a cutoff distance of 2.40 Å between hydrogen and acceptor and no angle cutoff. A hydrogen bond was considered to be present if it displayed occupancy >0.2, where occupancy is defined as the number of frames in which the bond occurs divided by the total number of frames in a trajectory.

Covariance calculations

Covariance analysis was performed to identify correlations between protein motions throughout the simulation. The correlation ($C_{i,j}$) between two

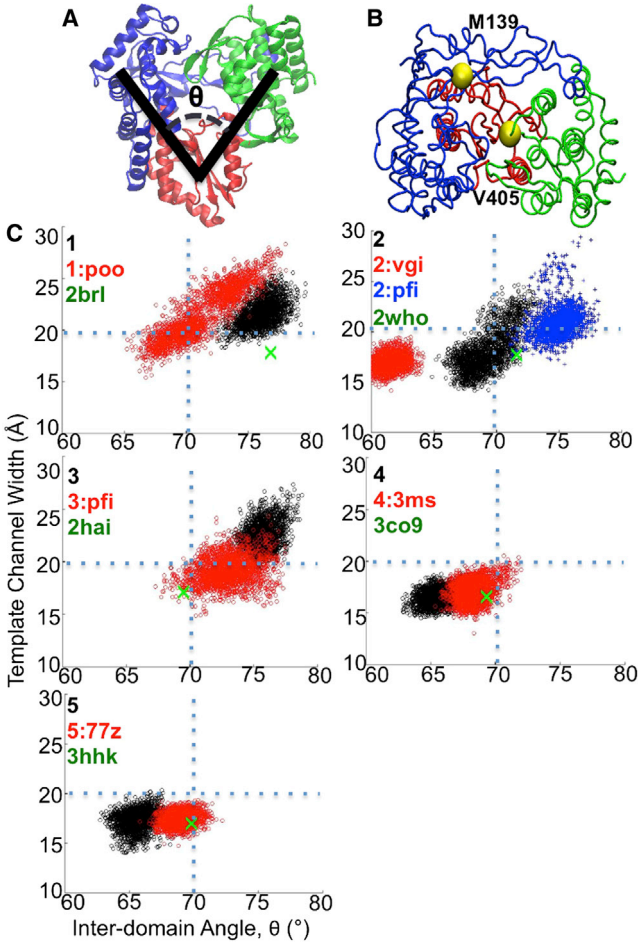

FIGURE 2 Plots of interdomain angle (θ) and template channel width demonstrate changes in enzyme conformation upon ligand binding. (*A*) The value θ is calculated by measuring the angle between the centers of mass of each domain. (*B*) The template channel width is calculated by measuring the distance between the centers of mass of residues 139 and 405 (indicated by *yellow spheres*). (*C*) θ (*x* axis) versus template channel width (*y* axis) for each system. Smaller angles and narrower widths correspond to a more closed enzyme. Values of 70° for θ and 20 Å for the template channel width (*green lines* in the plots) represent the demarcation between open and closed conformations. (*Black circles*) Snapshots from the free enzyme simulations; (*red* or *blue circles*) ligand-bound snapshots; (*green X* on each plot) original x-ray crystal structures. To see this figure in color, go online.

atoms i and j is determined by calculating the dot product between the differences of each atom's current position (r_i) from its average position ($\langle r_i \rangle$) using the CORREL module of the software CHARMM (http://www.charmm.org/):

$$C_{i,j} = \frac{\langle (r_i - \langle r_i \rangle) \cdot (r_j - \langle r_j \rangle) \rangle}{\sqrt{\langle (r_i - \langle r_i \rangle)^2 \rangle \langle (r_j - \langle r_j \rangle)^2 \rangle}}. \quad (3)$$

The most significant changes in correlated motion upon ligand binding are observed for 1/1:POO (see Fig. S3) and 2/2:VGI (28). In the former, presence of POO increases the extent of correlated motions, while the presence of VGI decreases correlated motions.

NETWORKVIEW plug-in: critical residues

The NETWORKVIEW plug-in for VMD (41) was used to identify residues likely to be critical for allosteric communication in NS5B. To begin, trajectories containing the centers of mass of each residue and the ligand (if present in that system) were generated. These were analyzed to generate an allosteric communication network. Networks are sets of nodes in which pairs of nodes are connected by edges. In this analysis, each center of mass is considered a node. Two nodes are connected by an edge if the nodes are within 8.5 Å of each other for at least 75% of the trajectory. Residues adjacent in sequence are excluded and cannot be connected by an edge. Edges are weighted according to the correlation between residues as computed via Eq. 3. Path-lengths between distant nodes are calculated by summing the edge weights between consecutive nodes along a path and the shortest path distance between all pairs of nodes in the network is evaluated using the Floyd-Warshall algorithm. The betweenness of an edge is measured by calculating the number of shortest paths that cross that edge. The Girvan-Newman algorithm (42) was used to calculate communities in the network, which are collections of nodes that have more connections to other nodes in the community than to any other node outside the community. Allosteric communication is thought to occur preferentially over edges between two communities with the greatest betweenness. Pairs of residues connected by such edges are considered critical residues.

RESULTS AND DISCUSSION

We performed a total of nine simulations: four with free enzyme and five with a ligand bound (three thumb-bound and two palm-bound structures). In addition, results from a previous set of simulations including an NNI-2 inhibitor are included here for completeness (28). We confirmed that the ligands remained bound to the enzyme throughout the simulations via visual inspection of each trajectory. Fig. 1 shows the structures of each ligand and their corresponding IC_{50} values (19,21–24).

Overall, ligand binding shifts the conformational sampling of the enzyme compared to the free structures, which is demonstrated by the distributions of interdomain angles (θ) and template channel widths shown in Fig. 2. Panels *A* and *B* in Fig. 2 illustrate how θ and the template channel width are calculated. Panel *C* shows the conformation sampled by various free structures (indicated by a single number, e.g., 1), ligand-bound structures (a number followed by a colon and the ligand identifier, e.g., 1:POO), and the respective original crystal structure given by the PDB codes (all PDB codes used are listed in Table 1). The changes in conformation upon ligand binding are accompanied by changes in enzyme flexibility, hydrogen bonding, and correlated motions, demonstrating that the structural and dynamic effects of ligand binding propagate throughout the entire enzyme and impact diverse enzyme properties.

Thumb site I (NNI-1) inhibitors reduce enzyme stability

The NNI-1 binding site is at the intersection of the Δ1 loop (residues 25–35) and rear of the thumb domain on

NS5B (see Figs. 1 and 3). Inhibitors binding to this site were originally referred to as "finger-loop" inhibitors (43) and are thought to prevent initiation of RNA replication (19). NNI-1 ligands disrupt a number of hydrogen bonds between the fingers and thumb domains and interact with the protein via hydrophobic interactions (19). Several researchers suggest that ligand binding at this site disrupts vital communication between the Δ1 loop and thumb domain, locking the enzyme into an open conformation (19). These suggestions are due in part to the similarity of NNI-1 bound structures to that of NS5B from genotype 2a (PDB: 1YV2), which is thought to be in the open conformation (19,39). While our simulations do indicate that the NNI-1 inhibitor disrupts communication between the Δ1 loop and thumb domain, we do not observe that the enzyme becomes trapped in an open conformation. Instead, our results indicate that the NNI-1-bound enzyme is unable to stably adopt either open or closed conformations, because it rapidly samples conformations with average θ-values and template channel widths of 74° and 25 Å, and 69° and 20 Å, respectively.

Fig. 2 compares conformations sampled in the free and ligand-bound structures. Simulation 1 samples an open conformation for 91% of the analyzed simulation. However, 1:POO mostly fluctuates between open (56%) and closed (28%) conformations. We believe that the increased conformational diversity observed in 1:POO is caused by the disruption of hydrogen bonds between the Δ1 loop and the thumb domain by POO as shown in Fig. 3. In addition to the large-scale conformational changes, the local flexibility of 1:POO is altered, which can be seen in the Δ*RMSF* plots in Fig. 4. While residues within the fingers domain involved in ligand binding become more rigid in 1:POO, most other regions of the protein (residues: ~100, ~150, ~405, ~450, and ~515) become more flexible compared to 1. The flexibility of these regions suggests that 1:POO is intrinsically less stable than 1. Residues in the vicinity of positions 100 and 400 in the enzyme participate in anti-correlated motions for 1:POO (see Fig. S3), which are associated with opening and closing of the fingers and thumb domains. This motion is observed in the lowest frequency mode derived from principal component analysis and is provided as Movie S4 in the Supporting Material.

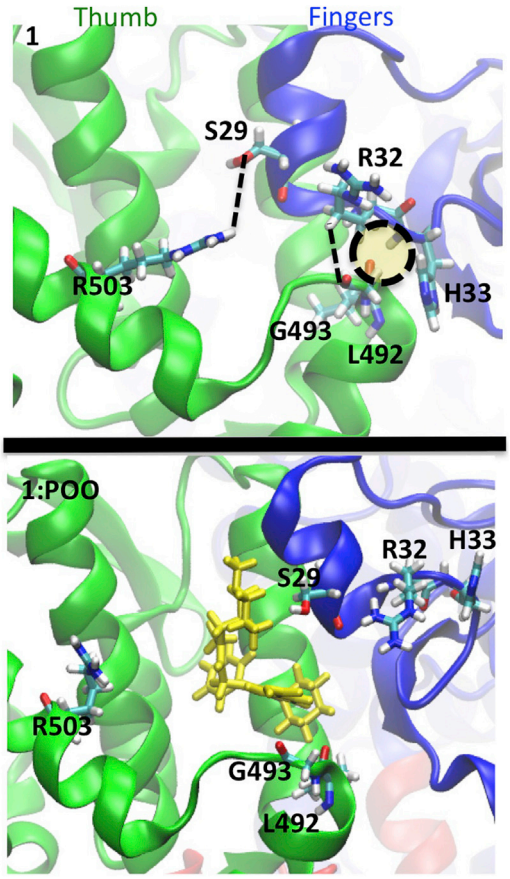

FIGURE 3 NNI-1 binding site displaying key hydrogen bonds between the fingers and thumb domains. (*Upper panel*) The free structure; (*lower panel*) ligand-bound structure. The hydrogen bond between residue H33 and L492 (occupancy of 80%) in 1 is disrupted upon ligand binding. Hydrogen bonds between residues S29 and R503 and between R32 and G493 also occur in most of the other structures, with occupancies ranging from 20 to 80%. To see this figure in color, go online.

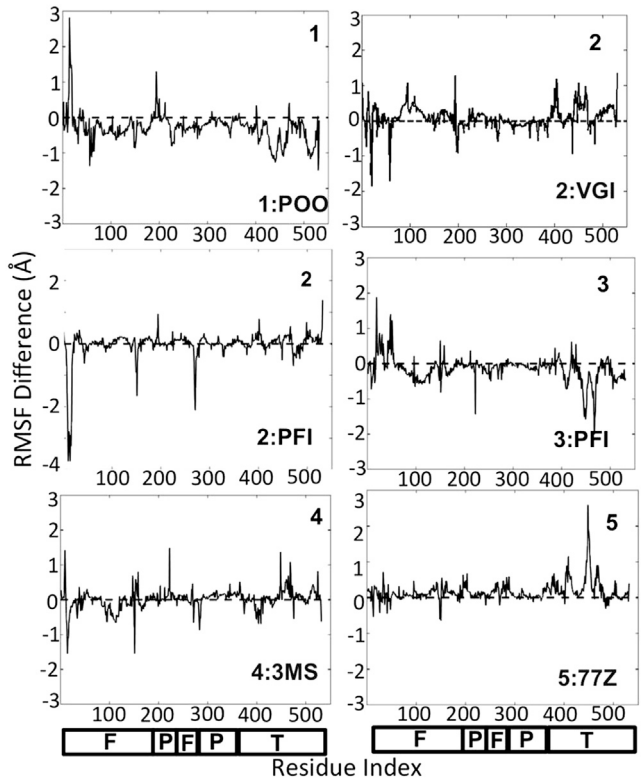

FIGURE 4 Δ*RMSF* plots. Peaks above zero indicate residues that are more flexible in the free enzyme, while peaks below zero indicate residues that are more flexible in the ligand-bound enzyme. The bars at the bottom of the plot indicate the locations of the fingers (F), palm (P), and thumb (T) domains.

Overall, the motion of the thumb domain is disconnected from the rest of the enzyme, because it no longer interacts with the Δ1 loop. This suggests that the Δ1 loop is no longer able to regulate transitions between open and closed conformations, which is in contrast to what we observed in our previous studies of the free enzyme (9) and to the suggestions of Di Marco et al. (19) and Labonté et al. (44). The divergent observations in these studies of 1:POO and previous investigations may result from the impact of POO in destabilizing the enzyme and disrupting allosteric communication pathways between the Δ1 loop and thumb domain. This possibility could be tested by using amino-acid substitutions to disrupt such interactions in the free enzyme, to replicate the effects of having an NNI-1 ligand present. For example, our simulations indicate that residues S29, R32, and H33 in the Δ1 loop form hydrogen bonds with the thumb domain (Fig. 3) and might be good choices to mutate in order to mimic the behavior of an NNI-1 ligand. Similar mutations L30S and L30R were generated by Labonté et al. (44). Both mutated enzymes were found to be inactive and unable to incorporate nucleotides into RNA transcripts.

The continuous sampling of several different conformations that we observe during our MD simulations is not necessarily inconsistent with the predictions made by Di Marco et al. (19) that the enzyme is locked in an open conformation by NNI-1 inhibitors. These authors may have observed only one of the two conformational minima that we see in our studies. This enzyme could be trapped in the more open state in their work due to crystal-packing effects. In addition, as noted in Materials and Methods, the PDB: 2BRL structure used for 1:POO contains a loop with missing residues (22,29–34). The coordinates of these residues were inserted by employing the corresponding coordinates from the PDB: 2WHO structure. It is possible that this flexible loop adopts a different conformation in our simulations than actually present in the PDB: 2BRL crystal structure. However, we believe the loop conformation present in our simulations is accurate because it was energy-minimized in the context of the known coordinates before simulations for 1:POO were initiated. In addition, these residues were subjected to long periods of molecular dynamics to allow for equilibration before any analysis was performed. The fact that ligand binding at the NNI-1 site compromises the enzyme's ability to stably occupy the open and closed conformations would likely prevent the enzyme from stabilizing initiation or elongation complexes during replication.

Thumb site II (NNI-2) inhibitors reduce conformational sampling

The NNI-2 binding site is located at the base of the thumb domain (Fig. 1) and NNI-2 ligands are thought to inhibit an initiation step of RNA synthesis (13,21,23). In a previous study that examined 2 and 2:VGI, we found that the NNI-2 ligand VGI induces a hyperclosed conformation that we do not believe to be replication-competent (28). The enzyme appeared to be trapped in this state and thus prevented from sampling other conformations. The hyperclosed conformation was stabilized by hydrogen bonds between the fingers and thumb domains that are also present in closed conformations observed in this study (see discussion below).

In this work, another crystal structure (PDB: 2HAI, system 3 in Table 1) with a different inhibitor (PFI) in the same thumb binding site as VGI (NNI-2) was simulated to determine whether these structurally different ligands (Fig. 2) induce the same hyperclosed conformation. In addition, PFI bound to the free structure generated previously (2:PFI in Table 1) was simulated to control for the possible impact of mutations in system 3 on its structure and dynamics. These mutations are all found in the fingers domain and also occur in the NS5B from genotype 2a of HCV. These are among several amino-acid changes that differentiate genotype 2a from 1b, providing an opportunity to begin to understand how different genotypes might respond to the presence of inhibitors.

Our simulations suggest that PFI induces conformations in both 2:PFI and 3:PFI that exhibit similar characteristics (see Fig. S5). Thus, PFI induces similar conformations regardless of enzyme sequence, suggesting that the ligand is primarily responsible for the conformations observed and not the three-point mutations in system 3 compared to system 2. Hydrogen-bond analysis confirms that PFI has the same interactions with the protein in both 2:PFI and 3:PFI, which is consistent with both PFI-bound enzymes sampling conformational distributions that largely overlap (see Fig. S5). A smaller template channel width is the main characteristic that differentiates 2:PFI (75% open conformation) and 3:PFI (96% open and intermediate conformations) from system 3, which samples an open conformation for 100% of the analyzed simulation. Both PFI-bound structures sample conformations that are more open compared to system 2 from our previous study (see Fig. 2). System 2 mostly samples a closed conformation (63%) and spends only 16% of the simulation in an open conformation.

As previously mentioned, VGI induced a hyperclosed conformation in 2:VGI not observed for 2:PFI or 3:PFI, even though it binds to the same binding site (NNI-2). The observation that PFI and VGI bind to the same NNI-2 site yet induce different conformational states is quite remarkable and unanticipated. This suggests that the unique local interactions between the ligand and protein are responsible for different global effects. Hydrogen bonds involving residues S476 and Y477 are thought to be important for the potency of ligands in this binding site (13). Hydrogen-bond analysis reveals that neither ligand forms a hydrogen bond

with Y477 over the course of the simulations. However, VGI forms a direct hydrogen bond with S476 while PFI does not, instead forming a direct hydrogen bond with R501. It is possible that this difference plays a role in inhibitor potency, because VGI has a lower IC_{50} value than PFI. In either case, ligand binding disrupts the local hydrogen-bonding network, which could propagate to induce the global changes observed. The differences in inhibitor potency for VGI and PFI may also relate to the degree to which each ligand induces closed conformations. This is consistent with the results of our simulations, with the more potent VGI-producing conformations that are on average more closed than those induced by PFI. Ligand potency could also be related to the extent by which enzyme motions are decreased due to the ligands, with VGI inducing more dramatic reductions in NS5B motions than PFI (see Figs. 4 and S3).

Palm site I (NNI-3) Inhibitors limit conformational sampling and block access of the RNA template

The NNI-3 binding site is at the intersection of the palm and thumb domains adjacent to the active site (Fig. 1). The two NNI-3 inhibitors examined in this study have similar scaffolds and engage in hydrophobic interactions and hydrogen bonds with all three domains of NS5B. Similar types of inhibitors have been identified for other viral polymerases (Dengue, herpes, and pestiviruses), suggesting that this site provides an effective means of inhibiting polymerase function in many viruses (45).

In contrast to systems 1 and 3, both systems 4 and 5 sample fully closed conformations for 100% of the analyzed simulation (see Fig. 2). Hydrogen bonds between the carbonyl oxygen of L91 and amino hydrogen of C451, as well as between the guanidinium group of R109 and the carbonyl oxygen of D444, are formed for both systems 4 and 5 and help stabilize the closed state (see Fig. 5). These hydrogen bonds are also observed in the hyperclosed conformation, but with opposite patterns of occupancy (28). Although they still sample closed conformations, the ligand-bound systems 4:3MS and 5:77Z sample conformations that are more open than those sampled by systems 4 and 5 (see Fig. 2). The ligand-bound structures also display different patterns of hydrogen bonds. Neither palm-bound system exhibits the hydrogen bond between L91 and C451 and only 4:3MS achieves the hydrogen bonds between R109 and D444 observed for systems 4 and 5. In addition, the two inhibitors form hydrogen bonds that are unique to each system: 3MS with N291 and 77Z with Y448. These differences in hydrogen bonding could be due to the slight variation in ligand structure between 3MS and 77Z (see Fig. 1). Despite these differences, both ligands appear to induce similar structural and dynamic changes in PDB: NS5B. As shown in Fig. 2, both 3MS and 77Z lock the enzyme into partially closed conformations and prevent the enzyme from sampling other conformational states.

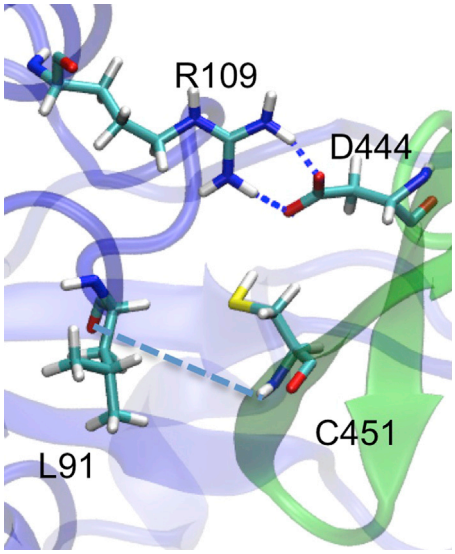

FIGURE 5 Hydrogen bonds that differentiate enzyme conformations. In fully closed conformations the hydrogen bonds between R109 and D444 have occupancies of ~80% while the hydrogen bond between L91 and C451 has an occupancy of ~20%. In the hyperclosed conformation, the pattern is reversed: the hydrogen bonds between R109 and D444 have occupancies of ~20% and the hydrogen bond between L91 and C451 has an occupancy ~80%. To see this figure in color, go online.

Palm inhibitors have been suggested to prevent the initiation of replication by physically blocking access of template RNA and incoming NTPs to the active site (13). Results from our simulations are consistent with this observation. Structural alignments of average structures taken from our simulations of 4:3MS or 5:77Z with a template-enzyme complex (PDB: 1NB7) indicate that palm inhibitors stably occupy locations that would hinder the template from accessing the catalytic site. This effect should significantly diminish enzyme activity (see Fig. 6 for 4:3MS).

The free enzyme can assume open conformations suitable for elongation

Free enzymes that were generated from crystal structures containing inhibitors bound to the thumb domain (systems 1–3) predominantly sampled conformations that were more open than their corresponding ligand-bound structures. However, both systems 1 and 3 sample conformations that are even more open than system 2. Fig. S6 shows prototypical structures that represent the spectrum of conformations sampled by the different simulations, including the open conformation sampled by system 3. The RMSD values between these structures are provided in Table S7 in the Supporting Material.

While the fully closed conformation may favor initiation, the open conformation observed for systems 1 and 3 may be

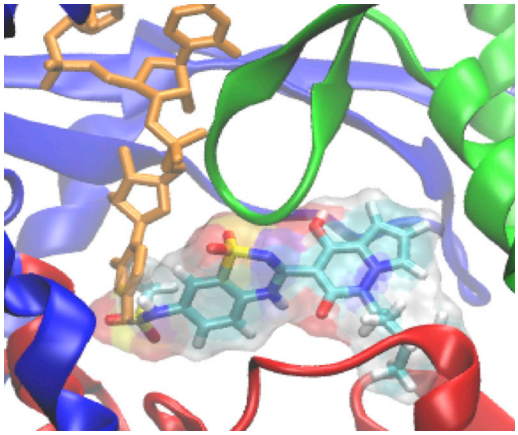

FIGURE 6 NNI-3 ligands obstruct the RNA template. Structural alignment between the average structure from 4:3MS and x-ray structure PDB: 1NB7 containing a short template strand. It is apparent that the path of the template to the active site would be blocked by the presence of the ligand. To see this figure in color, go online.

suitable for elongation. Although the presence of this state has been inferred based on the structural requirements for replication, to our knowledge, it has not previously been observed in molecular detail. It is possible that the 400-ns simulations performed for system 2 in our earlier studies were too short compared to the much longer simulations for systems 1 and 3 (at least 700 ns; see Table 1) for this state to be observed in that work (28). In the open conformation observed for systems 1 and 3, the fingers and thumb domains have rotated away from each other as shown in the average structures (Fig. S6). The average θ and duplex channel widths for systems 1 and 3 are (76.1°, 21.1 Å) and (75.7°, 22.2 Å), respectively. In contrast, a crystal structure of NS5B from genotype 2, previously classified as open (PDB: 1YV2), has an angle of 71.5° and a duplex channel width of 17.3 Å (39). Similarly, a structure of the related RNA polymerase from Poliovirus (PDB: 3OL6) that contains double-stranded RNA displays a duplex channel width of 18.6 Å (37). Because they contain duplex channels that are even wider than those observed for PDB: 1YV2 and PDB: 3OL6, the open conformations observed for systems 1 and 3 should be able to readily accommodate double-stranded RNA and should be well suited for elongation of the RNA strand.

Inhibitor binding can disrupt long-range communication within PDB:NS5B

We generated network graphs to represent the communication pathways in the enzyme using the NETWORKVIEW plugin for VMD (41) (see Materials and Methods). This analysis was performed to understand how long-range communication between residues in the enzyme changes upon ligand binding. While differences exist, there are several regions with similar collections of critical residues among the different systems. In particular, there are changes to community organization upon ligand binding. Fig. S8 shows the differences in community composition between 1 and 1:POO. The changes are representative of the manner in which ligand binding affects community composition. The ligand is able to induce effects distal to its binding site, as illustrated by the fact that communities in the fingers domain also change upon POO binding (see Fig. S8).

The large number of critical residues in each system suggests that allosteric communication can occur along many different pathways. If such communication is functionally significant, this occurrence may have implications in allowing the enzyme to become resistant to allosteric inhibitors. While binding of allosteric inhibitors may abolish some of these communication pathways, there may be other routes within the enzyme that can also fulfill these roles.

Table S9 lists the number of communities and critical residues identified for each system and the location of these residues within different structural motifs of NS5B. In most cases, NS5B has a larger number of critical residues when it is bound to thumb inhibitors than when it is free of ligand. The increase in critical residues is due to an increased number of communities, which indicates that the enzyme dynamics as a whole is less cohesive. Thus, in general, there is a lower level of globally coupled dynamics in the presence of thumb inhibitors. The only exception to this is 2:PFI. In general, PFI does not alter the dynamics of the enzyme as much as the other inhibitors.

In contrast, the palm inhibitors induce varying effects when compared to their free enzyme counterparts. While 3MS reduces the number of communities and critical residues, 77Z increases the number of communities and critical residues. Thus, the influence on enzyme dynamics appears to differ based on specific interactions formed between the enzyme and these ligands.

Critical residues highlight functional roles of structural motifs

Fig. S10 shows the locations of the different motifs and functional regions on the enzyme structure. All systems have critical residues in motif F as well as functional region II. Both motifs are important for template binding. Most systems have critical residues in motif B and functional regions III. Motifs B and F also play a role in NTP binding, while functional region III is required to bind the nascent RNA strand. The observation that all or most systems have critical residues in these regions suggests that these residues occur along allosteric pathways that mediate allosteric effects in both free and ligand-bound states.

While critical residues that are common to multiple enzyme systems may be of fundamental importance to numerous functional properties, critical residues that occur only in distinct conformations may be important for specific functional roles performed in that state. As a case in point,

all free enzymes that sampled closed conformations had critical residues in functional region I or motif G. Both regions are located at the top of the fingers domain lining the template channel and are responsible for RNA template binding.

These results allow us to hypothesize why residues in specific regions may be critical. Critical residues in regions involved in template binding (i.e., motifs B, F, and G and functional regions I and II) may signal to other enzyme regions that template recognition has occurred in the closed conformation. In contrast, critical residues in regions involved in binding of the nascent RNA strand (motif E and functional region III) may signal the transition to the open conformation to allow the double-stranded RNA to exit the enzyme. There was not a trend observed for motifs A, C, D, and E, which play roles in catalysis. This may be because the simulations did not contain template RNA bound to the enzyme, and thus would not be expected to sample conformations or engage in patterns of dynamics directly relevant to the catalytic event.

CONCLUSIONS

Our observations provide insight into the mechanisms of inhibition mediated by three distinct allosteric binding sites of the HCV RNA polymerase NS5B. We find that ligands at each of the three sites induce distinct patterns of conformational sampling and enzyme flexibility. The NNI-1 inhibitor destabilizes the enzyme by disrupting key interactions between the fingers and thumb domains, preventing conformations necessary for function from being stably occupied. In contrast, NNI-2 inhibitors reduce conformational sampling of the enzyme, locking it into either a more closed or a more open conformation, depending on the specific inhibitor in question. The NNI-3 inhibitors are similar to NNI-2 inhibitors in that they also restrict the conformational sampling of the enzyme, although both of the inhibitors studied in this work lock the enzyme into more open conformations relative to the free enzyme. In addition, NNI-3 inhibitors may prevent the RNA template from accessing the active site. Given that the binding site for NNI-4 inhibitors partially overlaps that of NNI-3 inhibitors, it is likely that the observations made for NNI-3 inhibitors will also apply to NNI-4. In summary, we have observed that allosteric inhibitors likely prevent polymerase function through three mechanisms: 1) eliminating transitions between the two major functional conformations (the closed conformation required for initiation and the open conformation required for elongation), 2) destabilizing the enzyme and preventing it from stably sampling functional conformations, and 3) preventing the RNA template from accessing the active site.

In addition to illuminating the molecular mechanisms by which allosteric inhibitors may alter functional properties of the HCV polymerase, our findings inform us about the fundamental functional properties of the enzyme. Specifically, we observe that conformations likely to be suitable for the initiation and elongation of RNA replication can occur in the free enzyme. Systems 4 and 5 sampled closed conformations suitable for the initiation of replication while systems 1 and 3 sampled open conformations that may readily accommodate double-stranded RNA present during elongation.

The graph theoretic analysis afforded by the NETWORKVIEW plugin for VMD (41) provides insight into how allosteric inhibitors alter long-range communication networks in PDB: NS5B. With this knowledge it should be possible to alter the function of the enzyme in well-defined ways via amino-acid substitution targeted to critical residues. For example, it should be possible to generate enzymes with native dynamics even in the presence of inhibitor (i.e., a resistant enzyme). It should also be possible to generate enzymes with perturbed dynamics in the absence of an inhibitor. We are in the process of performing such studies.

Many viral polymerases such as HIV-RT and 3D-pol from poliovirus share similar structural and dynamic elements with NS5B. Thus, the knowledge gained in this study may be relevant to understanding the intrinsic functional properties of a large number of viral polymerases, as well as how to alter the function of these and other enzymes via small molecules.

SUPPORTING MATERIAL

Supporting Materials and Methods, eight figures, four tables, and one movie are available at http://www.biophysj.org/biophysj/supplemental/S0006-3495(15)00234-9.

AUTHOR CONTRIBUTIONS

I.F.T. and B.C.D. designed the research; B.C.D. and J.A.B. performed the research and analyzed the data; and I.F.T., B.C.D., and J.A.B. wrote the article.

ACKNOWLEDGMENTS

The hardware used in the computational studies is part of the University of Maryland, Baltimore County High Performance Computing Facility.

The facility is supported by the U.S. National Science Foundation through the Major Research Instrumentation program (grant Nos. CNS-0821258 and CNS-1228778) and the Scientific Computing Research Environments for the Mathematical Sciences program (grant no. DMS-0821311), with additional substantial support from the University of Maryland, Baltimore County. This work also used the Extreme Science and Engineering Discovery Environment (XSEDE), which is supported by National Science Foundation grant number ACI-1053575. In addition, B.D. and J.B. were funded by National Institutes of Health NIH-F31 grants (Nos. GM106959-01 and GM106958-01, respectively).

SUPPORTING CITATIONS

Reference (46) appears in the Supporting Material.

REFERENCES

1. McHutchison, J. G., R. Bartenschlager, …, J. M. Pawlotsky. 2006. The face of future hepatitis C antiviral drug development: recent biological and virologic advances and their translation to drug development and clinical practice. *J. Hepatol.* 44:411–421.
2. World Health Organization. June 2011. Hepatitis C Fact Sheet No. 164. http://www.who.int/mediacentre/factsheets/fs164/en/.
3. Lindenbach, B. D., and C. M. Rice. 2005. Unraveling hepatitis C virus replication from genome to function. *Nature.* 436:933–938.
4. Ortín, J., and F. Parra. 2006. Structure and function of RNA replication. *Annu. Rev. Microbiol.* 60:305–326.
5. Walker, M. P., and Z. Hong. 2002. HCV RNA-dependent RNA polymerase as a target for antiviral development. *Curr. Opin. Pharmacol.* 2:534–540.
6. Ng, K. K.-S., J. J. Arnold, and C. E. Cameron. 2008. Structure-function relationships among RNA-dependent RNA polymerases. *Curr. Top. Microbiol. Immunol.* 320:137–156.
7. Chinnaswamy, S., I. Yarbrough, …, C. C. Kao. 2008. A locking mechanism regulates RNA synthesis and host protein interaction by the hepatitis C virus polymerase. *J. Biol. Chem.* 283:20535–20546.
8. van Dijk, A. A., E. V. Makeyev, and D. H. Bamford. 2004. Initiation of viral RNA-dependent RNA polymerization. *J. Gen. Virol.* 85:1077–1093.
9. Davis, B. C., and I. F. Thorpe. 2013. Molecular simulations illuminate the role of regulatory components of the RNA polymerase from the hepatitis C virus in influencing protein structure and dynamics. *Biochemistry.* 52:4541–4552.
10. Butcher, S. J., J. M. Grimes, …, D. I. Stuart. 2001. A mechanism for initiating RNA-dependent RNA polymerization. *Nature.* 410:235–240.
11. Adachi, T., H. Ago, …, K. Yatsunami. 2002. The essential role of C-terminal residues in regulating the activity of hepatitis C virus RNA-dependent RNA polymerase. *Biochim. Biophys. Acta.* 1601:38–48.
12. Condon, S. M., M. G. LaPorte, and T. Herbertz. 2005. Allosteric inhibitors of hepatitis C NS5B RNA-dependent RNA polymerase. *Curr. Med. Chem.* 4:99–110.
13. Beaulieu, P. 2009. Recent advances in the development of NS5B polymerase inhibitors for the treatment of hepatitis C virus infection. *Expert Opin. Ther. Pat.* 49:145–164.
14. Beaulieu, P. L., and Y. S. Tsantrizos. 2004. Inhibitors of the HCV NS5B polymerase: new hope for the treatment of hepatitis C infections. *Curr. Opin. Investig. Drugs.* 5:838–850.
15. Beaulieu, P. L. 2009. Recent advances in the development of NS5B polymerase inhibitors for the treatment of hepatitis C virus infection. *Expert Opin. Ther. Pat.* 19:145–164.
16. Biswal, B. K., M. Wang, …, M. N. G. James. 2006. Non-nucleoside inhibitors binding to hepatitis C virus NS5B polymerase reveal a novel mechanism of inhibition. *J. Mol. Biol.* 361:33–45.
17. Caillet-Saguy, C., P. C. Simister, and S. Bressanelli. 2011. An objective assessment of conformational variability in complexes of hepatitis C virus polymerase with non-nucleoside inhibitors. *J. Mol. Biol.* 414:370–384.
18. de Vicente, J., R. T. Hendricks, …, R. Farrell. 2009. Non-nucleoside inhibitors of HCV polymerase NS5B. Part 4: structure-based design, synthesis, and biological evaluation of benzo[d]isothiazole-1,1-dioxides. *Bioorg. Med. Chem. Lett.* 19:5652–5656.
19. Di Marco, S., C. Volpari, …, A. Carfí. 2005. Interdomain communication in hepatitis C virus polymerase abolished by small molecule inhibitors bound to a novel allosteric site. *J. Biol. Chem.* 280:29765–29770.
20. Hendricks, R. T., S. R. Spencer, …, S. Swallow. 2009. 3-Hydroxyisoquinolines as inhibitors of HCV NS5b RNA-dependent RNA polymerase. *Bioorg. Med. Chem. Lett.* 19:410–414.
21. Li, H., J. Tatlock, …, S. Fuhrman. 2006. Identification and structure-based optimization of novel dihydropyrones as potent HCV RNA polymerase inhibitors. *Bioorg. Med. Chem. Lett.* 16:4834–4838.
22. Ruebsam, F., S. E. Webber, …, L. Kirkovsky. 2008. Pyrrolo[1,2-b]pyridazin-2-ones as potent inhibitors of HCV NS5B polymerase. *Bioorg. Med. Chem. Lett.* 18:3616–3621.
23. Ontoria, J. M., E. H. Rydberg, …, A. Carfì. 2009. Identification and biological evaluation of a series of 1H-benzo[de]isoquinoline-1,3(2H)-diones as hepatitis C virus NS5B polymerase inhibitors. *J. Med. Chem.* 52:5217–5227.
24. Shaw, A. N., R. Tedesco, …, M. N. Zimmerman. 2009. Substituted benzothiadizine inhibitors of hepatitis C virus polymerase. *Bioorg. Med. Chem. Lett.* 19:4350–4353.
25. Nyanguile, O., F. Pauwels, …, P. Raboisson. 2008. 1,5-benzodiazepines, a novel class of hepatitis C virus polymerase nonnucleoside inhibitors. *Antimicrob. Agents Chemother.* 52:4420–4431.
26. Nyanguile, O., B. Devogelaere, …, G. C. Fanning. 2010. 1a/1b Subtype profiling of nonnucleoside polymerase inhibitors of hepatitis C virus. *J. Virol.* 84:2923–2934.
27. Tomei, L., S. Altamura, …, G. Migliaccio. 2003. Mechanism of action and antiviral activity of benzimidazole-based allosteric inhibitors of the hepatitis C virus RNA-dependent RNA polymerase. *J. Virol.* 77:13225–13231.
28. Davis, B. C., and I. F. Thorpe. 2013. Thumb inhibitor binding eliminates functionally important dynamics in the hepatitis C virus RNA polymerase. *Proteins.* 81:40–52.
29. Vanommeslaeghe, K., E. Hatcher, …, A. D. MacKerell, Jr. 2010. CHARMM general force field: a force field for drug-like molecules compatible with the CHARMM all-atom additive biological force fields. *J. Comput. Chem.* 31:671–690.
30. Jorgensen, W. L., J. Chandrasekhar, …, M. L. Klein. 1983. Comparison of simple potential function for simulating liquid water. *J. Phys. Chem.* 79:926–935.
31. Vanommeslaeghe, K., and A. D. MacKerell, Jr. 2012. Automation of the CHARMM general force field (CGenFF) I: bond perception and atom typing. *J. Chem. Inf. Model.* 52:3144–3154.
32. Vanommeslaeghe, K., E. P. Raman, and A. D. MacKerell, Jr. 2012. Automation of the CHARMM general force field (CGenFF) II: assignment of bonded parameters and partial atomic charges. *J. Chem. Inf. Model.* 52:3155–3168.
33. Phillips, J. C., R. Braun, …, K. Schulten. 2005. Scalable molecular dynamics with NAMD. *J. Comput. Chem.* 26:1781–1802.
34. Maragliano, L., and E. Vanden-Eijnden. 2006. A temperature accelerated method for sampling free energy and determining reaction pathways in rare events simulations. *Chem. Phys. Lett.* 426:168–175.
35. Abrams, C. F., and E. Vanden-Eijnden. 2010. Large-scale conformational sampling of proteins using temperature-accelerated molecular dynamics. *Proc. Natl. Acad. Sci. USA.* 107:4961–4966.
36. Lesburg, C. A., M. B. Cable, …, P. C. Weber. 1999. Crystal structure of the RNA-dependent RNA polymerase from hepatitis C virus reveals a fully encircled active site. *Nat. Struct. Biol.* 6:937–943.
37. Gong, P., and O. B. Peersen. 2010. Structural basis for active site closure by the poliovirus RNA-dependent RNA polymerase. *Proc. Natl. Acad. Sci. USA.* 107:22505–22510.
38. Moustafa, I. M., H. Shen, …, C. E. Cameron. 2011. Molecular dynamics simulations of viral RNA polymerases link conserved and correlated motions of functional elements to fidelity. *J. Mol. Biol.* 410:159–181.
39. Biswal, B. K., M. M. Cherney, …, M. N. G. James. 2005. Crystal structures of the RNA-dependent RNA polymerase genotype 2a of hepatitis C virus reveal two conformations and suggest mechanisms of inhibition by non-nucleoside inhibitors. *J. Biol. Chem.* 280:18202–18210.
40. Schmitt, M., N. Scrima, …, S. Bressanelli. 2011. A comprehensive structure-function comparison of hepatitis C virus strain JFH1 and J6 polymerases reveals a key residue stimulating replication in cell culture across genotypes. *J. Virol.* 85:2565–2581.
41. Eargle, J., and Z. Luthey-Schulten. 2012. NETWORKVIEW: 3D display and analysis of protein•RNA interaction networks. *Bioinformatics.* 28:3000–3001.

42. Girvan, M., and M. E. Newman. 2002. Community structure in social and biological networks. *Proc. Natl. Acad. Sci. USA*. 99:7821–7826.

43. Hirashima, S., T. Suzuki, …, H. Hashimoto. 2006. Benzimidazole derivatives bearing substituted biphenyls as hepatitis C virus NS5B RNA-dependent RNA polymerase inhibitors: structure-activity relationship studies and identification of a potent and highly selective inhibitor JTK-109. *J. Med. Chem.* 49:4721–4736.

44. Labonté, P., V. Axelrod, …, P. Mak. 2002. Modulation of hepatitis C virus RNA-dependent RNA polymerase activity by structure-based site-directed mutagenesis. *J. Biol. Chem.* 277:38838–38846.

45. Garriga, D., C. Ferrer-Orta, …, N. Verdaguer. 2013. Role of motif B loop in allosteric regulation of RNA-dependent RNA polymerization activity. *J. Mol. Biol.* 425:2279–2287.

46. Copyright (c) 1996–2007 Grace Development Team.